ACS APPLIED MATERIALS & INTERFACES

Research Article

www.acsami.org

A Novel Nanomaterial of Graphene Oxide Dotted with Ni Nanoparticles Produced by Supercritical CO_2-Assisted Deposition for Reducing Friction and Wear

Yuan Meng, Fenghua Su,* and Yangzhi Chen

School of Mechanical and Automotive Engineering, South China University of Technology, Guangzhou 510640, People's Republic of China

Supporting Information

ABSTRACT: Graphene oxide dotted with nickel nanoparticles (Sc−Ni/GO) was synthesized by chemical deposition with the assistance of supercritical carbon dioxide ($scCO_2$). The deposited Ni nanoparticles with diameters less than 5 nm are uniformly anchored on the surfaces of GO nanosheets. The as-prepared Sc−Ni/GO composites were employed as lubricating additives in paraffin oil and their tribological properties were tested using a four-ball tribometer. The results demonstrate that the Sc−Ni/GO composites are efficient lubricant additives. Adding 0.08 wt % Sc−Ni/GO into paraffin oil can reduce the friction coefficient and wear scar diameter by 32 and 42%, respectively, in comparison with the pure oil. In addition, Sc−Ni/GO composites exhibit superior lubricating performances than nano-Ni, GO nanosheets, and Ni/GO composites produced without the aid of $scCO_2$. Such excellent lubricating properties of the Sc−Ni/GO composites derive from the synergistic lubricating actions of Ni nanoparticles and GO nanosheets during the rubbing process. The synergistic lubricating actions are closely related to the microstructure of the nanocomposites and the characteristic features of transfer film formed on the contact steel balls. The anchored Ni nanoparticles with smaller size and more uniform distribution on GO surfaces and the thin transfer film formed on the contact balls favor the full play of the synergistic actions.

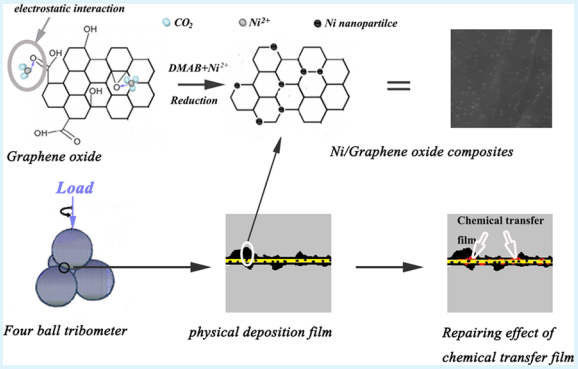

KEYWORDS: *graphene, nickel, nanomaterial, friction and wear, supercritical CO_2*

1. INTRODUCTION

Graphene has drawn great research and industrial attention mainly in the past decade due to its unique electrical, optical, thermal, and mechanical properties. It also has been demonstrated to be an effective solid lubricant and lubricating additive.[1−8] Eswaraiah et al.[1] found that the ultrathin graphene significantly improved the lubricating performance of the engine oil. Frictional characteristics, antiwear abilities, and extreme pressure properties of the graphene dispersed oil were improved by 80, 33, and 40% respectively, compared with the base oil. Berman et al.[2] reported that solution-processed graphene layers reduced friction and wear on sliding steel surfaces in air. They thought that the graphene layers could act as a two-dimentional nanomaterial and formed a conformal protective coating on the sliding contact interfaces, facilitating shear, slowing the tribo-corrosion and, hence, drastically reducing the wear.

Recently, graphene and graphene oxide have been authenticated as ideal substrates to load nanoparticles, such as silver (Ag), gold (Au), platinum (Pt), and so on, onto their nanosheet surfaces, owing to their low surface energy and high loading capacity.[9−20] Nguyen et al.[9] prepared Ag nanoparticle-decorated graphene composites by a simple hydrogen reduction of silver precursor. Muszynski et al.[10] produced nano-Au/graphene composites using a solution-based approach of chemical reduction of $AuCl_4$-ions in graphene suspensions. Not only the laminated graphene oxide is a good supporter to decorate metal nanoparticles but also the as-prepared nanocomposites exhibit much better performance than the individual graphene or nanoparticles. Zhao et al.[11] found that the prepared PtRu/GO composites possess better electrocatalytic reactivity than the individual PtRu nanoparticles. As a type of soft metal nanomaterial, the magnetic nickel (Ni) nanoparticles have attracted a great deal of research attention as a lubricating additive because of its low cost, facile preparation, and self-repairing activity.[21,22] Chen et al.[21] demonstrated that monodispersed Ni nanoparticles greatly improved the antiwear behavior of the filled poly alpha-olefin (PAO6) oil, even at a low concentration of 0.05 wt %. We believe that once Ni nanoparticles are introduced onto the nanosheets of graphene oxide, the as-prepared Ni/GO nanocomposites will achieve better lubricating performance than that of individual nano-Ni

Received: March 26, 2015
Accepted: May 18, 2015
Published: May 18, 2015

DOI: 10.1021/acsami.5b02650
ACS Appl. Mater. Interfaces 2015, 7, 11604−11612

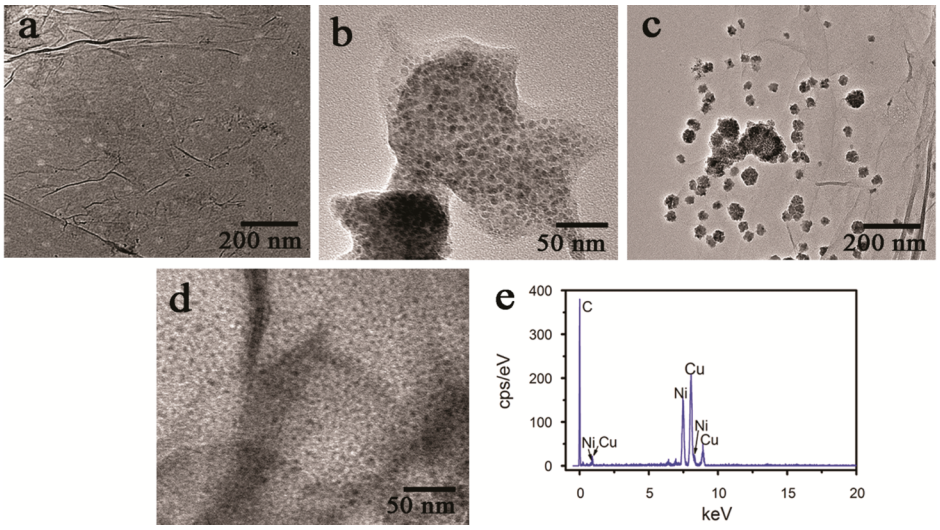

Figure 1. TEM images of (a) GO, (b) nano-Ni, (c) Ni/GO composites, and (d) Sc−Ni/GO composites; and (e) EDX spectrum of Sc−Ni/GO composites in panel d.

or GO because their synergistic friction-reducing and antiwear potentials may occur.

Despite all kinds of nanoparticles have been decorated on GO nanosheets, it is still a great challenge to achieve homogeneous foreign materials with even size distribution on the GO nanosheet surfaces because of the easy agglomerating and restacking tendency of GO nanosheets. Supercritical carbon dioxide ($scCO_2$) has many distinctive properties, including excellent mass-transfer capability, gas-like diffusivity, and extremely low viscosity, and thus, it is applicable to uniformly disperse nanoparticles onto the high-surface-energy supporting materials.[23−25] Some previous results have confirmed that the nanoparticles synthesized with assistance of $scCO_2$ possess smaller and more homogeneous sizes and better distribution on substrates than the ones produced without the aid of $scCO_2$.[26−28] Moreover, these works have shown that the as-prepared nanocomposites with the aid of $scCO_2$ exhibit superior properties in their practical applications. For example, Chen et al.[26] found that highly dispersed Pd nanoparticles could be directly decorated on carbon nanotubes with the aid of $scCO_2$. The as-prepared composites demonstrated much better activity toward hydrogen spillover compared to those fabricated without the aid of $scCO_2$.

Here, we provide a facile chemical deposition for the controllable synthesis of Ni nanoparticles/GO nanosheets composites (Sc−Ni/GO) with the aid of $scCO_2$. The resulting nanocomposites are employed as lubricating additives in paraffin oil and their tribological properties are systemically investigated using a four-ball tribometer. For references, the samples of GO, nano-Ni, and Ni/GO composites prepared in air are also produced and studied. Finally, the synergistic lubricating mechanisms of Ni nanoparticles and GO nanosheets in the Sc−Ni/GO composites are proposed by analyzing the worn surfaces on the tested balls.

2. EXPERIMENTAL SECTION

2.1. Materials. Natural graphite (average size ∼44 μm) was supplied from Qingdao Dongkai Co., Ltd., of China. $NaNO_3$ and $KMnO_4$ were supplied from Sino Pharm Chemical Reagent Co., Ltd., of China. Sodium dodecyl sulfate (SDS), oleic acid, and sodium citrate (A.R. > 99.9%) were purchased from Tianjin Fuchen Chemical Reagent Factory of China. $NiCl_2·6H_2O$ (A.R. 99%) was supplied from Jinan Shenghe Chemical Industry Co., Ltd. of China. The reducing agent was dimethyl amineborane (DMAB; A.R. > 98.5%), which was purchased from Shanghai Hansi Chemical Co., Ltd., of China. All chemicals used were of analytical grade.

2.2. Synthesis of GO and GO-based Nanocomposites. In this work, GO was synthesized from natural graphite powders using a modified Hummers method.[29,30] The details were provided in the Supporting Information. $NiCl_2·6H_2O$ was used as the precursor for the syntheses of nano-Ni and Ni/GO nanocomposites. To prepare Sc−Ni/GO composites, 100 mg of $NiCl_2·6H_2O$, 5 mg of sodium dodecyl sulfate (SDS) and 2.5 mg of sodium citrate were first codissolved in 60 mL of ethanol with magnetic stirring. After that, 100 mg of GO and 75 mg of DMAB were added into the mixed solution one by one, and the mixed solution was subsequently treated with ultrasonic vibration for 10 min. Then, the mixed solution was loaded in a 100 mL stainless autoclave. After that, pressurized CO_2 was introduced into the system under heating conditions. The supercritical state of CO_2 was achieved when the pressure and temperature reached 18 MPa and 100 °C, respectively. Figure S1 (SI) schematically presents the $scCO_2$-assisting deposition system. The mixed solution in the system was vigorously magnetically stirred to facilitate the completion of the reaction and generate homogeneous product. After 2 h, the system was depressurized and slowly cooled to room temperature. The resulting products were isolated by centrifugation and then repeatedly washed with copious distilled water and ethanol. The Ni nanoparticles were also synthesized using the same method without the addition of GO. In addition, the Ni/GO nanocomposites were produced by traditional chemical deposition. The operation process and parameters were similar to those for producing Sc−Ni/GO nanocomposites without the assistance of $scCO_2$.

2.3. Sample Characterizations. The morphologies of the prepared samples were examined using high-resolution transmission electron microscopy (TEM, JEOL JEM-2010F) and field-emission scanning electron microscopy (FESEM, JEOL JSM 6700F). The elemental composition information was obtained by Energy Dispersive X-ray Detector attached TEM from the same image for TEM analysis. The phase structures were studied by X-ray diffractometer (XRD, Bruker D8 advance) with a Cu Ka radiation (1.5405 Å). The X-ray detector was scanned at a rate of 0.5 per minute from diffraction angle of 5−80°. Thermogravimetric analysis (TGA) was performed from room temperature to 1000 °C at a heating rate of 10 °C per minute in a protective atmosphere of N_2. Raman spectra were recorded using a RENISHAW inVia instrument with excitation energies of 514.5 nm and 20 mW. Fourier transform infrared (FTIR) spectra were recorded on a Nicolet Nexus 670 FT-IR Spectrometer in the range of 400−4000 cm^{-1}.

DOI: 10.1021/acsami.5b02650
ACS Appl. Mater. Interfaces 2015, 7, 11604−11612

2.4. Friction and Wear Behaviors. To improve the dispersibility of the as-prepared nanomaterial in paraffin oil, we treated 0.1 g nanomaterial (GO or nano-Ni, Ni/GO, Sc−Ni/GO) with 10 mL oleic acid under magnetic stirring at 80 °C for 1 h. After that, the mixture was washed with copious ethanol to remove extra oleic acid and dried at 80 °C for 2 h to obtain the oleic acid-modified nanomaterial. Before tribo-test, the oleic-acid-modified nanomaterial with desirable content was dispersed in paraffin oil under ultrasonication for 30 min for producing the nanomaterial dispersed oil. The tribological properties of the pure paraffin oil and the nanomaterial dispersed oils were tested by a four-ball tribometer (MRS-10A, Jinan Yihua Tribology Testing Technology Co., Ltd. China). The used balls with diameter of 12.7 mm and surface roughness of 0.020 μm were composed of GCr15 bearing steel. The hardness of the balls is 61−65 HRC. The tests were performed at room temperature and ambient humidity for 30 min under different loadings (50−300 N) and rotating speeds (300−1500 rpm). After testing, the steel balls were ultrasonically cleaned in petroleum ether and dried in air. The wear scar diameter (WSD) on the tested ball was measured by an optical microscopy (107JA; Shanghai Changfang Optical Instrument Co., Ltd., China), and each scar was measured at least three times under the same conditions to ensure standard deviations less than 5%. The morphologies and chemical compositions of the worn surfaces were determined by field-emission scanning electron microscopy (FESEM, JEOL JSM 6700F) and X-ray photoelectron spectroscopy (XPS, Kratos Axis Ultra DLD).

3. RESULTS AND DISCUSSION

3.1. Morphology and Microstructure. TEM images of GO, nano-Ni, Ni/GO, and Sc−Ni/GO are shown in Figure 1. It can be observed that the GO nanosheets are super thin and transparent with some wrinkles on the surface (Figure 1a). As shown in Figure 1b, nano-Ni possesses a globose microstructure with an average diameter of 5−10 nm. To identify the role of $scCO_2$ in the synthesis of the composites, TEM images of Ni/GO and Sc−Ni/GO are shown in Figure 1c,d. It is clear that the morphologies and the distributions of the dotted Ni nanoparticles are totally different in the two samples. Figure 1c (without $ssCO_2$) shows coarser Ni nanoparticles, which evidently tend to join together and agglomerate, leading to massive clusters on GO sheets. The introduction of $scCO_2$ significantly improves the microstructures of the dotted Ni nanoparticles on GO sheets. As shown in Figure 1d, the GO nanosheets are anchored with highly dispersed Ni nanoparticles with uniform diameters less than 5 nm. The EDX spectrum of the Sc−Ni/GO from its TEM image is shown in Figure 1e. Strong Ni peaks are observed, suggesting that the Ni nanoparticles are successfully anchored on GO nanosheet surfaces. Note that the strong Cu peaks derive from the copper grid for TEM analysis.

Figure 2 shows the SEM images of these samples. Figure 2a further confirms that GO sheets are transparent with very thin thickness and a few wrinkles. The morphologies of the Ni nanoparticles after drying from their dispersion are shown in Figure 2b. Although most of the nanoparticles join together to form network clusters due to the drying process, a few globose and grainy nanoparticles are still observed in the clusters. By comparing panels c and d in Figure 2, the findings from TEM analyses can be reinforced. For the Ni/GO sample, the diameter distribution ranges of the Ni nanoparticles are very wide. A few Ni nanoparticles on GO sheets disperse poorly and form big clusters. However, for the Sc−Ni/GO sample, the Ni nanoparticles with uniform diameter size are homogeneously decorated on GO nanosheet surfaces. In general, the deposited Ni nanoparticles with high-quality distribution are achieved without any surface pretreatment for GO for the Sc−Ni/GO nanocomposites. $ScCO_2$ possesses a variety of excellent characters such as gas-like viscosity, enhanced transport efficiency, and small surface tension, which is very helpful for the wetting of GO sheets and the adhesion of Ni ions to the GO surfaces. In addition, the miscibility between ethanol and $scCO_2$ can enhance the dissolving capacity of $scCO_2$ and baffle the escape of Sc−Ni/GO caused by depressurizing and releasing CO_2.

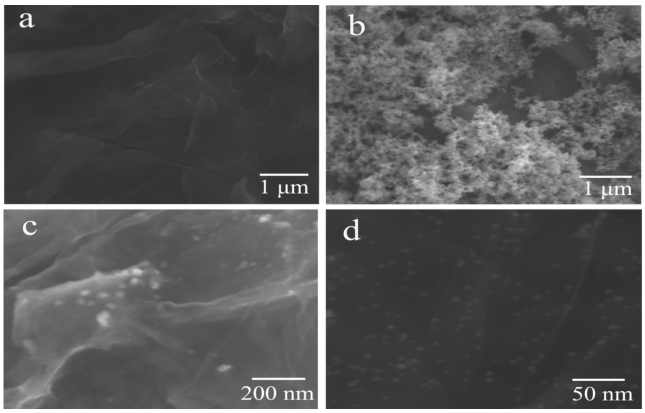

Figure 2. SEM images of (a) GO, (b) nano-Ni, (c) Ni/GO composites, and (d) Sc−Ni/GO composites.

Figure 3a shows the FT-IR spectra of GO, Ni/GO and Sc−Ni/GO samples. The typical peaks of GO at 3410 cm^{-1} (stretching vibration of C−OH), 1730 cm^{-1} (C═O), and 1400 cm^{-1} (deformation vibration of C−OH) are clearly observed for the GO sample. And the peak at 1630 cm^{-1} is attributed to the skeletal vibration of graphitic skeleton and the peak at 1060 cm^{-1} confirms the existence of C−O−C in the GO sample. Interestingly, the peak at 1730 cm^{-1} disappears and the peaks at 3410 cm^{-1}, 1400 and 1060 cm^{-1} are still observed for the Ni/GO and Sc−Ni/GO nanocomposites. These results show that the reduction reactions indeed occur during the synthesis process of Ni/GO and Sc−Ni/GO nanocomposites. But, the reduction of GO is mild and incomplete, evidenced by the existences of C−O−C and C−OH in the two samples. The Raman spectra of GO, Ni/GO, and Sc−Ni/GO samples are shown in Figure 3b. When compared to the GO sample, the nanocomposites of Ni/GO and Sc−Ni/GO exhibit slightly higher ratio of D band intensity to G band intensity (I_D/I_G). The increase of I_D/I_G is mainly due to the increase of defects on GO surface and the decrease of relative dimension of GO sheets. The increasing defects and decreasing dimension of GO nanosheets in the two nanocomposites might originate from the anchoring of Ni nanoparticles on the GO surfaces. In addition, the linear shape in the Raman spectra between 300 and 1000 cm^{-1} (Figure 3b, inset) confirms no metallic oxides of Ni_2O_3 existing in the Ni/GO and Sc−Ni/GO nanocomposites.

XRD patterns of GO, nano-Ni, Ni/GO, and Sc−Ni/GO samples are shown in Figure 4a. In the pattern of the GO sample, the carbon (001) characteristic peak of graphite oxide is clearly observed at 10°. This peak becomes weaker and wider in the patterns of both Ni/GO and Sc−Ni/GO, which is attributed to the reduction of some oxidation groups on GO (Figure 3a) during the deposition process. Furthermore, the smooth carbon (002) diffraction peak appears in the patterns of the two nanocomposites. In the case of nano-Ni pattern, the peaks at 44.3, 51.7, and 76.1° are respectively assigned to (111),

DOI: 10.1021/acsami.5b02650
ACS Appl. Mater. Interfaces 2015, 7, 11604−11612

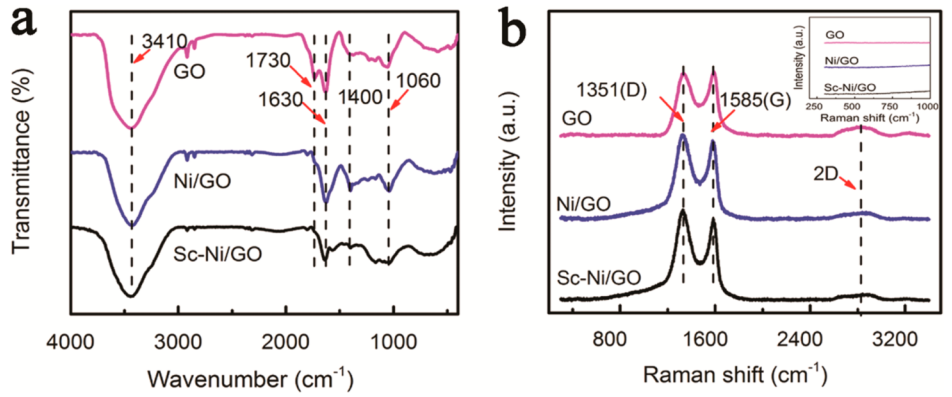

Figure 3. (a) FT-IR spectra and (b) Raman spectra of GO, Ni/GO, and Sc−Ni/GO samples; (b, inset) Raman spectra from 300 to 1000 cm^{-1}.

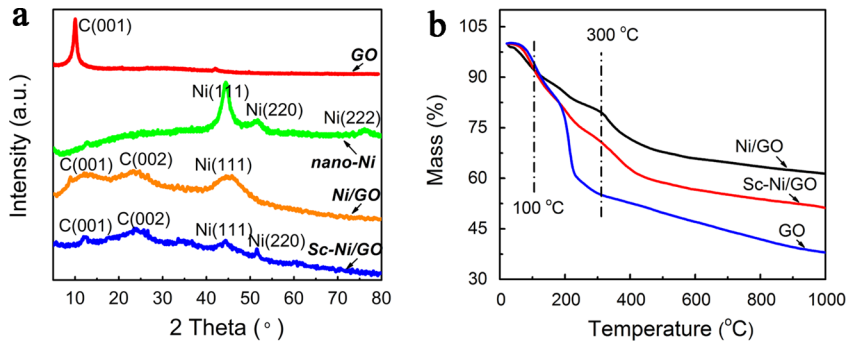

Figure 4. (a) XRD patterns of GO, nano-Ni, Ni/GO composites, and Sc−Ni/GO composites; (b) TGA curves of GO, Ni/GO composites, and Sc−Ni/GO composites.

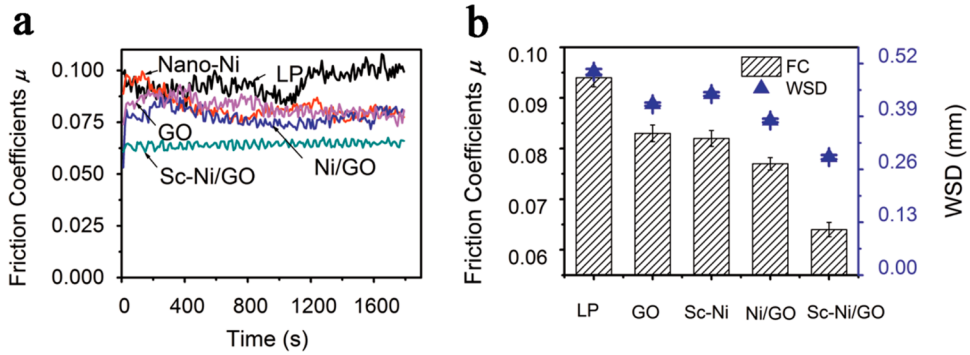

Figure 5. (a) Typical friction coefficient curves for the pure liquid paraffin oil (LP) and the dispersed oils with 0.08 wt % nano-Ni, GO, Ni/GO, and Sc−Ni/GO with increasing testing time. (b) Comparisons of the average friction coefficients and wear scar diameters (WSDs) of the balls lubricated with these oils (150 N, 900 rpm).

(200), and (220) crystalline planes of Nickel (JCPDS Card No.65-0380), which indicates that the Ni nanoparticles are face-centered cubic (fcc) structure. Interestingly, there is only Ni (111) peak in the pattern of Ni/GO and only Ni (111) and Ni (200) peaks in the pattern of Sc−Ni/GO, which might derive from the directional crystallization of Ni particles because of the enveloping by GO nanosheets. No peaks from other impurities are detected.

TGA curves of GO, Ni/GO and Sc−Ni/GO samples are shown in Figure 4b. For the GO sample, 5% weight loss below 100 °C is attributed to the removal of adsorbed water, and the main 40% weight loss within 100−300 °C is ascribed to the decomposition of labile oxygen functional groups.[29] There is also a steady weight loss of 17% between 400 and 1000 °C, which is assigned to the removal of more stable oxygen functionalities.[29] The total weight loss is around 62% for the GO sample when the temperature reaches 1000 °C. In contrast, the total weight loss of the Ni/GO composites and Sc−Ni/GO composites are respectively reduced to 39.6% and 45.4% at this temperature, which derives from the deposited Ni nanoparticles on the GO surfaces for the two composites. Meanwhile, the different weight loss between the Ni/GO and Sc−Ni/GO composites has close relation with the mass fractions of the deposited Ni nanoparticles in them. Although the Ni nanoparticles badly disperse and form big clusters in the Ni/GO composites (Figures 1c and 2c), the mass fraction of Ni nanoparticles is higher than that in the Sc−Ni/GO sample.

3.2. Tribology Properties. The stability of the nanomaterial dispersed oil greatly affects its lubricating performances. Figure S2 (SI) displays photographs of the base paraffin oil and

DOI: 10.1021/acsami.5b02650
ACS Appl. Mater. Interfaces 2015, 7, 11604−11612

the dispersed oil with 0.08 wt % GO, nano-Ni, Ni/GO, and Sc−Ni/GO after resting for 10 days. It is clear that the nanomaterial dispersed oils are stable without obvious precipitation behavior in the bottom of the bottles after resting a long time (10 days). Variations of friction coefficients of the base oil and the nanomaterial dispersed oils with increasing sliding time are shown in Figure 5a. These dispersed oils show smaller and more stable friction coefficients than the pure paraffin oil with the increase of sliding time. This result suggests that all these nanomaterials as a lubricating additive have positive functions for improving the friction property of the paraffin oil. However, these samples exhibit different friction-reducing efficiencies. The Sc−Ni/GO dispersed oil exhibits the lowest and the most stable friction coefficient, followed by the Ni/GO dispersed oil.

Comparisons of the average friction coefficients and the WSDs of the corresponding steel balls lubricated with these oils at 150 N and 900 rpm are shown in Figure 5b. All nanomaterials including GO, nano-Ni, Ni/GO and Sc−Ni/GO as additives can reduce the friction coefficients and the WSDs. The Sc−Ni/GO dispersed oil exhibits the lowest friction coefficient and the lowest WSD. Compared with the pure paraffin oil, the Sc−Ni/GO dispersed oil shows the friction coefficient and WSD reduced by 32% and 42%, respectively. Figure 5b also suggests that the nanocomposites of Sc−Ni/GO and Ni/GO as additives have better lubricating abilities than the individual nanomaterial of Ni or GO, which may derive from the synergistic lubricating actions of Ni nanoparticles and GO nanosheets in the composites. However, the better lubricating performances of Sc−Ni/GO than Ni/GO indicate that the synergistic lubricating potentials of nano-Ni and GO are closely related to the composite microstructure. As shown in Figures 1c and 2c, the anchored Ni nanoparticles on GO surfaces are coarser and featured with big size in the Ni/GO composites. But for the Sc−Ni/GO composites, the Ni nanoparticles with smaller diameters less than 5 nm are evenly dispersed on the GO nanosheet surfaces (Figures 1d and 2d). As a result, the antiwear and friction-reducing potentials of Ni nanoparticles and GO nanosheets are fully released and better synergistic effects can be achieved for the Sc−Ni/GO composites.

Figure 6 shows the friction coefficients and WSDs of the dispersed oil with varying concentrations of Sc−Ni/GO composites at 150 N and 900 rpm. It can be seen that traces of Sc−Ni/GO can evidently improve the lubricating properties of the paraffin oil. Although the variations of both the friction coefficients and WSDs exhibit a similar "deep valley" shape, the lowest friction coefficient appears at the concentration of 0.06 wt %, and the smallest WSD emerges at the concentration of 0.08 wt %. Therefore, the optimal concentration of Sc−Ni/GO composites in oil is 0.06−0.08 wt %. With this weight percentage, both friction coefficient and WSD values reach the lowest point, and the excellent lubricating performances of the dispersed oil are obtained.

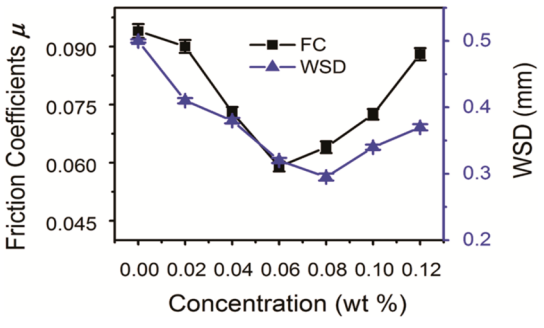

Figure 6. Variations of the friction coefficients and WSDs of the balls lubricated with the Sc−Ni/GO dispersed oil as a function of Sc−Ni/GO concentration at 150 N and 900 rpm.

Figure 7 describes the variations of the friction coefficients and WSDs of the balls lubricated with 0.08 wt % Sc−Ni/GO dispersed oil as a function of the loading and rotating speed. The loading and rotating speed have similar influences on the WSDs. The WSDs steadily increase with increasing loading and rotating speed. At first, the friction coefficient decreases and reaches a minimum value, and then it starts to increase with the sustainable increase of the loading and the rotating speed. There is a speedy decreasing phase for both of the two influence polylines of the friction coefficient. At this phase, the influences of loading and rotating speed start to get full play.

3.3. SEM and XPS Analyses of Wear Interfaces. Figure 8 shows the SEM images of the wear scar surfaces on the steel balls lubricated with these oils after sliding for 30 min at 150 N and 900 rpm. As shown in Figure 8a,b, the wear scar lubricated with the pure paraffin oil is the biggest one, and the wear surface is very rough. Many wide and deep furrows on the entire surface can be found, indicating that the metal-to-metal contact has occurred because of the poor lubrication of the pure oil. Adding Ni nanoparticles in oil slightly reduces the WSD on the ball (Figure 8c). Deep scratches and grooves still exist on this wear surface (Figure 8d), which indicates that the severe scuffing has occurred during the rubbing process. The steel ball lubricated with the GO dispersed oil shows a smooth wear surface, as shown in Figure 8e,f. The furrows on this wear surface become flat and smooth and the furrow numbers are also decreased. As shown in Figure 8g,i, the balls lubricated with the Ni/GO or Sc−Ni/GO dispersed oil display much smaller WSDs when compared to the ones lubricated with the dispersed oil with individual nano-Ni or GO. Moreover, their wear surfaces have less and shallower furrows and scratches (Figure 8h,j). The combinations of Ni and GO in composite indeed significantly develop the synergistic lubricating potentials as expected. However, there are still distinctions between the wear surfaces lubricated with the Ni/GO dispersed oil and the Sc−Ni/GO dispersed one (Figure 8g−j). The WSD lubricated with the Sc−Ni/GO dispersed oil (Figure 8i) is smaller than that lubricated with the Ni/GO dispersed oil (Figure 8g). And the wear scar surface lubricated with the Ni/GO dispersed oil is also featured with some adhesive wears as a result of a few scratches and grooves observed (Figures 8g,h). But the scratches and grooves become much shallower and thinner on the wear surface lubricated with the Sc−Ni/GO dispersed oil (Figure 8j). These results confirm that the Sc−Ni/GO composites are more effective than Ni/GO composites as lubricating additives. Some black remnants are observed in Figure 8j, indicating that a transfer film may form during the sliding process. XPS analyses were carried out to detect the chemical compositions of the transfer film for clarifying the tribochemical reactions during the sliding process.

XPS analyses of the wear scar on the ball lubricated with the Sc−Ni/GO dispersed oil were performed to explore the lubricating mechanism of this composite additive. Figure 9 shows the full spectrum (Figure 9a) from the binding energy of 0 (eV) to 1000 (eV) and the curve-fitted XPS spectra of C1s, O1s, Fe2p and Ni2p on the wear scar surface. The mass

DOI: 10.1021/acsami.5b02650
ACS Appl. Mater. Interfaces 2015, 7, 11604−11612

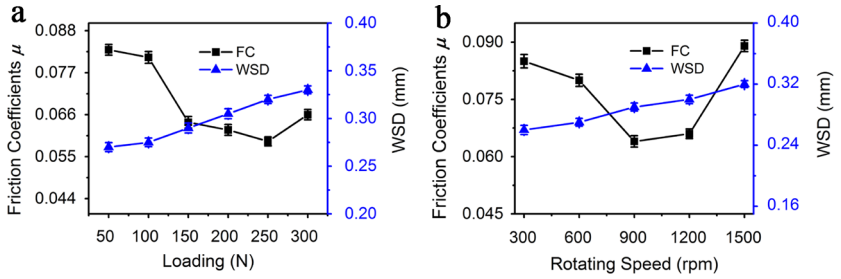

Figure 7. Variations of the friction coefficients and WSDs of the balls lubricated with 0.08 wt % Sc−Ni/GO dispersed oil as a function of (a) loading at 900 rpm and (b) rotating speed at 150 N.

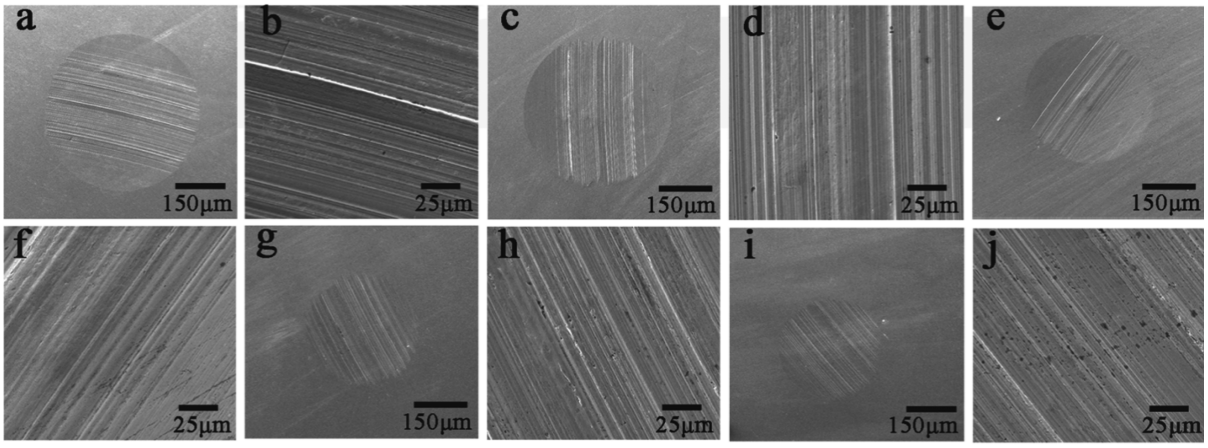

Figure 8. SEM images of the wear scar surfaces on the steel balls lubricated with the different oil samples after sliding for 30 min at 150 N and 900 rpm: (a and b) pure paraffin oil, (c and d) 0.08 wt % nano-Ni dispersed oil, (e and f) 0.08 wt % GO dispersed oil, (g and h) 0.08 wt % Ni/GO dispersed oil, and (i and j) 0.08 wt % Sc−Ni/GO dispersed oil.

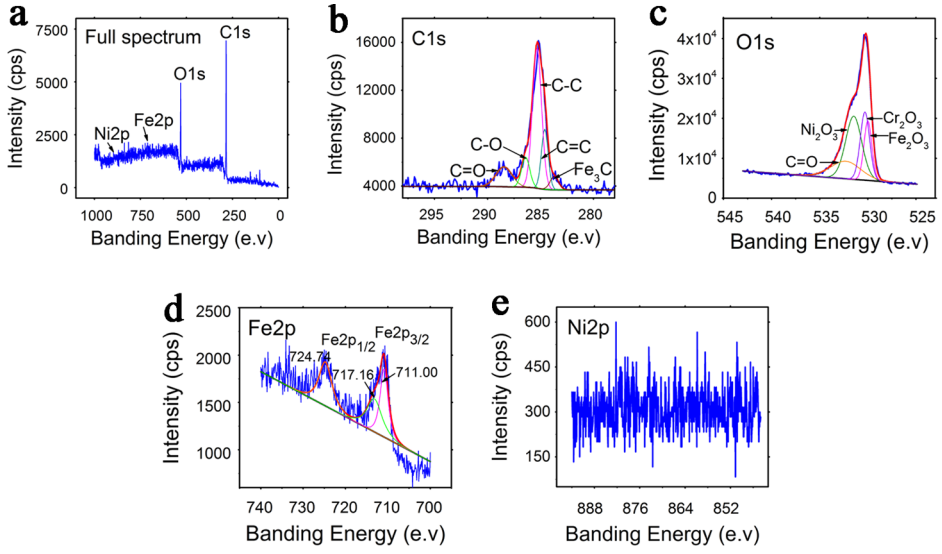

Figure 9. (a) XPS full spectrum and curve-fitted XPS spectra of (b) C1s, (c) O1s, (d) Fe2p, and (e) Ni2p on the wear scar surface of the ball lubricated with 0.08 wt % Sc−Ni/GO dispersed oil after sliding for 30 min at 150 N and 900 rpm.

fractions of the C, O, Fe and Ni elements, determined by XPS analysis, are listed in Table 1. As shown in Figure 9b, the Fe_3C signal is attributed to the intrinsic ingredient of cementite in the steel balls, while the C═O, C−O, C−C, C═C signals might originate from the Sc−Ni/GO composites. Furthermore, the mass fraction (27.10%) of C element on the wear scar surface (Table 1) is much higher than that in the GCr15 steel ball (0.95−1.05%). Therefore, we can reasonably conclude that the

Table 1. Relative Mass Fractions of Typical Elements on the Wear Scar Surface of the Ball Lubricated with 0.08 wt % Sc−Ni/GO Dispersed Oil after Sliding 30 min at 150 N and 900 rpm

element	C	O	Fe	Ni
mass fraction (wt %)	27.10	29.16	43.46	0.27

DOI: 10.1021/acsami.5b02650
ACS Appl. Mater. Interfaces 2015, 7, 11604−11612

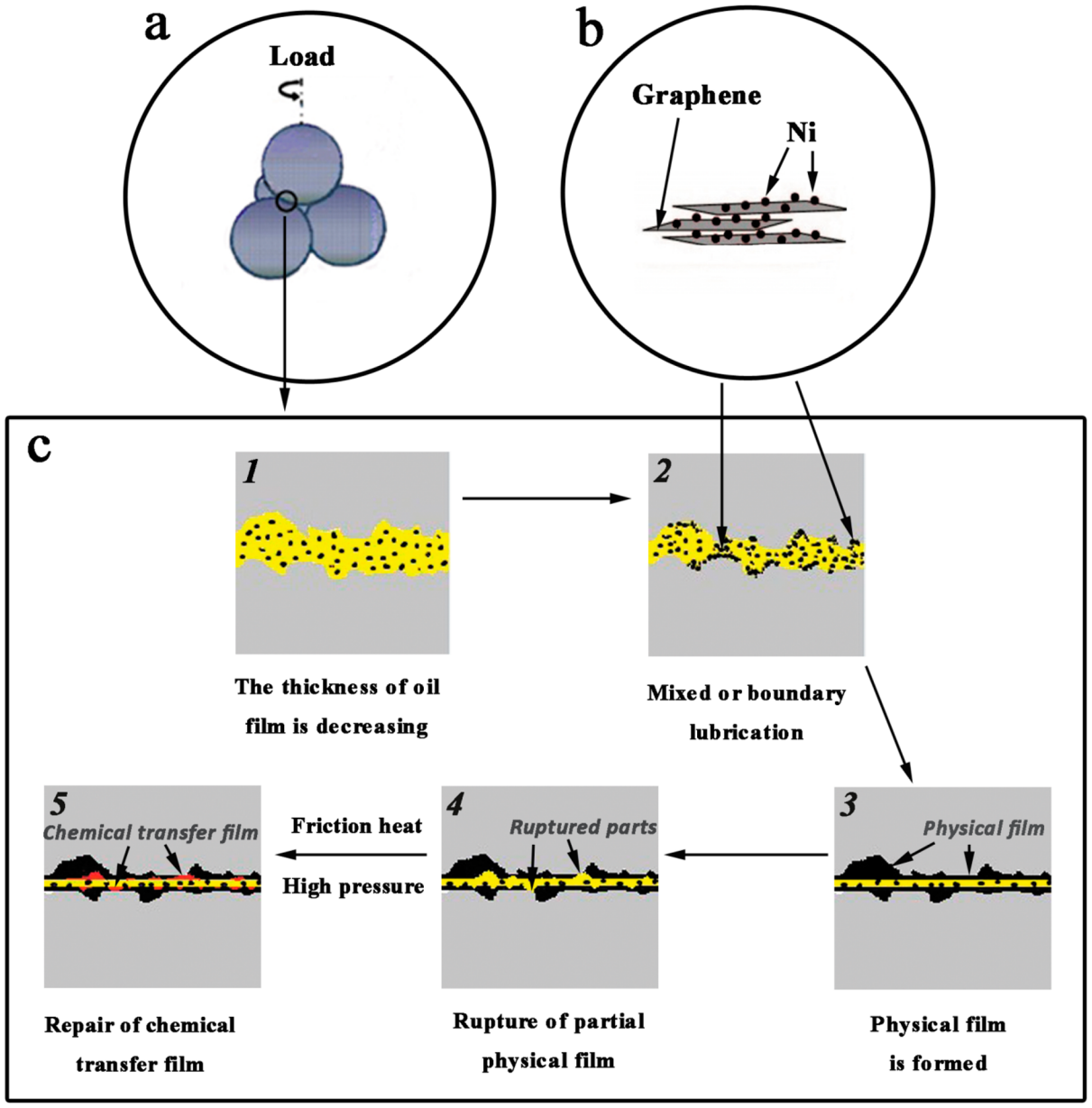

Figure 10. (a) Four-ball tribometer; (b) Sc−Ni/GO composite sheets; and (c) evolution of the transfer film formed on the interface of the contact balls lubricated with 0.08 wt % Sc−Ni/GO dispersed oil during the sliding process at 150 N and 900 rpm.

Sc−Ni/GO composites have been deposited on the contact surfaces and form a physical protecting film on the balls. This conclusion can be further authenticated by the Ni_2O_3 signal in O1s peak (Figure 9c) and the high mass ratio of Ni/Fe in the wear scar surface. As calculated from Table 1, the Ni/Fe mass ratio of 6.21/1000 on the scar surface is much higher than that of 3/1000 in the GCr15 steel. In addition, the C═O, C−O, and Ni_2O_3 signals also indicate that the Ni and C elements from the nanocomposites have reacted with oxygen during sliding process, resulting in a new chemical transfer film formed on the surface. Furthermore, the Fe_2O_3 signals in O1s peak (Figure 9c) and Fe2p peak (Figure 9d) suggest that a few Fe elements have been oxidized during the rubbing process. Because the mass fraction of Ni element is too low (0.27%) on the scar surface, no obvious peaks are shown in the XPS spectrum of Ni2p (Figure 9e).

3.4. Synergistic Lubricating Mechanism. Combining SEM and XPS analyses of the wear scar surfaces, we believe that the excellent lubricating performances of the Sc−Ni/GO composites originate from the synergistic lubricating actions of nano-Ni and GO. Figure 10a,b shows the schematic of the four-ball tribometer and the Sc−Ni/GO composite sheets, respectively. Figure 10c displays the evolution of the protecting film formed on the interface of the contact balls lubricated with the Sc−Ni/GO dispersed oil. At first, with the traction and compression created by high contact pressure, the Sc−Ni/GO composites penetrate into the interspace of the contact surfaces and gradually deposit in the original pits and valleys of these surfaces, resulting in the formation of a thin physical film. The GO sheets can fill up the pits and valleys and smooth the surface.[31,32] The Ni nanoparticles on the GO sheets reduce the restacking trend of GO and then prevent the damming actions of GO in the front edge of the interspace. These actions of Ni nanoparticles are advantageous to the formation of the thin physical film on the contact balls. The formed physical film is imparted with a lot important functions, including separating

DOI: 10.1021/acsami.5b02650
ACS Appl. Mater. Interfaces 2015, 7, 11604−11612

two mating metal surfaces to avoid direct contact, bearing the load from steel balls, and dispersing stress concentration.[33] As the test time goes on, the applied load at high rotating speed will produce high temperature and pressure. The thin physical film will be damaged, even totally broken, due to the produced high temperature and pressure. At the same time, the deposited GO and Ni nanoparticles the surfaces will undergo complex tribo-chemical reactions owing to the high temperature and pressure, resulting in the formation of a new chemical transfer film.[21] The formed chemical transfer film can supply the functions of the damaged physical film. Finally, the chemical transfer film completely replaces the physical film and has the role of reducing friction and wear. It is necessary to emphasize that the synergistic lubricating actions of Ni nanoparticles and GO nanosheets are closely related to the microstructures of the nanocomposites. The smaller size and more uniform distribution of Ni nanoparticles are more beneficial for bearing the load, dispersing stress concentration, and preventing the restacking of GO sheets. As a result, the Sc−Ni/GO is better than the Ni/GO as lubricating additives because of its better microstructures favoring the play of the synergistic actions of nano-Ni and GO in composites.

4. CONCLUSIONS

A facile one-step supercritical CO_2 chemical deposition route has been established to directly synthesize Sc−Ni/GO nanocomposites. Various characterizations confirm that the Ni nanoparticles with average diameters less than 5 nm are evenly anchored on the surfaces of the GO nanosheets. The lubricating performances of the synthesized Sc−Ni/GO nanocomposites as lubricating additives are much better than those of the individual GO, the individual nano-Ni and the Ni/GO nanocomposites produced without the aid of $scCO_2$. The 0.08 wt % Sc−Ni/GO dispersed oil displays the friction coefficient of 0.064 and the WSD of 0.29 mm that are reduced by 32 and 42%, respectively, compared to the pure oil. The results suggest that the Sc−Ni/GO nanocomposites have excellent lubricating performances and can be employed as efficient lubricating additives. The excellent lubricating performances of Sc−Ni/GO nanocomposites can be explained by the synergistic lubricating actions of Ni nanoparticles and GO nanosheets in the composites during the sliding process. The anchored Ni nanoparticles with smaller size and more uniform distribution favor the formation of a thin protecting film on the contact balls and can highly disperse the heavy load, which are sure to benefit the full play of the synergistic action. The findings here provide an alternative approach to fabricate nanocomposite as efficient lubricant additives, which hopefully will find real application soon.

■ ASSOCIATED CONTENT

Supporting Information

Synthesis of GO by modified Hummers method; schematic of the $scCO_2$-assisted deposition system for producing nanocomposites; and photographs of the pure oil and the nanomaterial dispersed oils. The Supporting Information is available free of charge on the ACS Publications website at DOI: 10.1021/acsami.5b02650.

■ AUTHOR INFORMATION

Corresponding Author

* E-mail: fhsu@scut.edu.cn. Tel./Fax.: +86-20-87112341.

Notes

The authors declare no competing financial interest.

■ ACKNOWLEDGMENTS

The authors are grateful to the National Natural Science Foundation of China (Grant no. 21473061) and the Fundamental Research Funds for the Central Universities (Grant no. 2014ZG0014) for financial support.

■ REFERENCES

(1) Eswaraiah, V.; Sankaranarayanan, V.; Ramaprabhu, S. Graphene-based Engine Oil Nanofluids for Tribological Applications. *ACS Appl. Mater. Interfaces.* **2011**, *3*, 4221−4227.
(2) Berman, D.; Erdemir, A.; Sumant, A. V. Few Layer Graphene to Reduce Wear and Friction on Sliding Steel Surfaces. *Carbon.* **2013**, *54*, 454−459.
(3) Liang, H.; Bu, Y.; Zhang, J.; Cao, Z.; Liang, A. Graphene Oxide Film as Solid Lubricant. *ACS Appl. Mater. Interfaces.* **2013**, *5*, 6369−6375.
(4) Khare, V.; Pham, M. Q.; Kumari, N.; Yoon, H. S.; Kim, C. S.; Park, J. I.; Ahn, S. H. Graphene−Ionic Liquid Based Hybrid Nanomaterials as Novel Lubricant for Low Friction and Wear. *ACS Appl. Mater. Interfaces.* **2013**, *5*, 4063−4075.
(5) Berman, D.; Erdemir, A.; Sumant, A. V. Graphene: A New Emerging Lubricant. *Mater. Today.* **2014**, *17*, 31−42.
(6) Egberts, P.; Han, G. H.; Liu, X. Z.; Johnson, A. T. C.; Carpick, R. W. Frictional Behavior of Atomically Thin Sheets: Hexagonal-Shaped Graphene Islands Grown on Copper by Chemical Vapor Deposition. *ACS Nano* **2014**, *8* (5), 5010−5021.
(7) Li, Y.; Wang, Q.; Wang, T.; Pan, G. Preparation and Tribological Properties of Graphene oxide/Nitrile Rubber Nanocomposites. *J. Mater. Sci.*. **2012**, *47*, 730−738.
(8) Hvizdoš, P.; Dusza, J.; Balázsi, C. Tribological Properties of Si_3N_4-Graphene Nanocomposites. *J. Eur. Ceram. Soc.*. **2013**, *33*, 2359−2364.
(9) Nguyen, V. H.; Kim, B.; Jo, Y.; Shim, J. Preparation and Antibacterial Activity of Silver Nanoparticles-Decorated Graphene Composites. *J. Supercrit. Fluids.* **2012**, *72*, 28−35.
(10) Muszynski, R.; Seger, B.; Kamat, P. V. Decorating Graphene Sheets with Gold Nanoparticles. *J. Phys. Chem. C* **2008**, *112*, 5263−5266.
(11) Zhao, J.; Xue, H.; Zhang, L.; Yu, J.; Hu, H. Decoration of Ultrafine Platinum-Ruthenium Particles on Functionalized Graphene Sheets in Supercritical Fluid and Their Electrocatalytic Property. *J. Nanopart. Res.* **2012**, *14*, 935−945.
(12) Shao, W.; Liu, X. F.; Min, H. H.; Dong, G. H.; Feng, Q. Y.; Zuo, S. L. Preparation, Characterization, and Antibacterial Activity of Silver Nanoparticle-Decorated Graphene Oxide Nanocomposite. *ACS Appl. Mater. Interfaces.* **2015**, *7* (12), 6966−6973.
(13) Tang, X.; Li, X.; Cao, Z.; Yang, J.; Wang, H.; Pu, X.; Yu, Z. Synthesis of Graphene Decorated with Silver Nanoparticles by Simultaneous Reduction of Graphene Oxide and Silver Ions with Glucose. *Carbon.* **2013**, *59*, 93−99.
(14) Mao, A.; Zhang, D.; Jin, X.; Gu, X.; Wei, X.; Yang, G.; Liu, X. Synthesis of Graphene Oxide Sheets Decorated by Silver Nanoparticles in Organic Phase and Their Catalytic Activity. *J. Phys. Chem. Solids.* **2012**, *73*, 982−986.
(15) Hong, W.; Bai, H.; Xu, Y.; Yao, Z.; Gu, Z.; Shi, G. Preparation of Gold Nanoparticle/Graphene Composites with Controlled Weight Contents and Their Application in Biosensors. *J. Phys. Chem. C* **2010**, *114*, 1822−1826.
(16) Wu, Z.; Ren, W.; Wen, L.; Gao, L.; Zhao, J.; Chen, Z.; Zhou, G.; Li, F.; Cheng, H. Graphene Anchored with Co_3O_4 Nanoparticles as Anode of Lithium Ion Batteries with Enhanced Reversible Capacity and Cyclic Performance. *ACS Nano* **2010**, *4* (6), 3187−3194.
(17) Si, Y.; Samulski, E. T. Exfoliated Graphene Separated by Platinum Nanoparticles. *Chem. Mater.*. **2008**, *20*, 6792−6797.

DOI: 10.1021/acsami.5b02650
ACS Appl. Mater. Interfaces 2015, 7, 11604−11612

(18) Sattayasamitsathit, S.; Gu, Y.; Kaufmann, K.; Jia, W.; Xiao, X.; Rodriguez, M.; Minteer, S.; Cha, J.; Burckel, D. B.; Wang, C.; Polsky, R.; Wang, J. Highly Ordered Multilayered 3D Graphene Decorated with Metal Nanoparticles. *J. Mater. Chem. A* **2013**, *1*, 1639−1645.
(19) Huang, C.; Pu, N.; Wang, C.; Huang, J.; Sung, Y.; Ger, M. Hydrogen Storage in Graphene Decorated with Pd and Pt Nano-Particles Using an Electroless Deposition Technique. *Sep. Purif. Technol.*. **2011**, *82*, 210−215.
(20) Hong, W.; Bai, H.; Xu, Y.; Yao, Z.; Gu, Z.; Shi, G. Preparation of Gold Nanoparticle/Graphene Composites with Controlled Weight Contents and Their Application in Biosensors. *J. Phys. Chem. C* **2010**, *114*, 1822−1826.
(21) Chen, Y.; Zhang, Y.; Zhang, S.; Yu, L.; Zhang, P.; Zhang, Z. Preparation of Nickel-Based Nanolubricants via a Facile in Situ One-Step Route and Investigation of Their Tribological Properties. *Tribol. Lett.*. **2013**, *51*, 73−83.
(22) Chou, R.; Battez, A. H.; Cabello, J. J.; Viesca, J. L.; Osorio, A.; Sagastume, A. Tribological Behavior of Polyalphaolefin with the Addition of Nickel Nanoparticles. *Tribol. Int.* **2010**, *43*, 2327−2332.
(23) Chen, C.; Lin, K.; Tsai, W.; Chang, J.; Tseng, C. Electroless Deposition of Ni Nanoparticles on Carbon Nanotubes with the Aid of Supercritical CO_2 Fluid and a Synergistic Hydrogen Storage Property of the Composite. *Int. J. Hydrogen Energy.* **2010**, *35*, 5490−5497.
(24) Bozbag, S. E.; Unal, U.; Kurykin, M. A.; Ayala, C. J.; Aindow, M.; Erkey, C. Thermodynamic Control of Metal Loading and Composition of Carbon Aerogel Supported Pt-Cu Alloy Nanoparticles by Supercritical Deposition. *J. Phys. Chem. C* **2013**, *117*, 6777−6787.
(25) Hiramatsu, M.; Hori, M. Preparation of Dispersed Platinum Nanoparticles on a Carbon Nanostructured Surface Using Supercritical Fluid Chemical Deposition. *Materials* **2010**, *3*, 1559−1572.
(26) Chen, C. Y.; Chang, J. K.; Tsai, W. T.; Hung, C. H. Uniform Dispersion of Pd Nanoparticles on Carbon Nanostructures Using a Supercritical Fluid Deposition Technique and Their Catalytic Performance towards Hydrogen Spillover. *J. Mater. Chem.*. **2011**, *21*, 19063−19068.
(27) Wu, J.-W.; Wang, C.-H.; Wang, Y.-C.; Chang, J.-K. Ionic-Liquid-Enhanced Glucose Sensing Ability of Non-enzymatic Au/Graphene Electrodes Fabricated Using Supercritical CO2 Fluid. *Biosens. Bioelectron.*. **2013**, *46*, 30−36.
(28) Lee, M.-T.; Fan, C.-Y.; Wang, Y.-C.; Li, H.-Y.; Chang, J.-K. Improved Supercapacitor Performance of MnO_2-Graphene Composites Constructed Using a Supercritical Fluid and Wrapped with an Ionic Liquid. *J. Mater. Chem.. A* **2013**, *1*, 3395−3405.
(29) Hummers, J. W. S.; Offeman, R. E. Preparation of Graphitic Oxide. *J. Am. Chem. Soc.*. **1958**, *80*, 1339−1339.
(30) Wu, T. T.; Ting, J. M. Preparation and Characteristics of Graphene Oxide and Its Thin Films. *Surf. Coat. Technol.*. **2013**, *231*, 487−491.
(31) Song, H. J.; Jia, X. H.; Li, N.; Yang, X. F.; Hua, T. Synthesis of α-Fe_2O_3 Nanorod/Graphene Oxide Composites and Their Tribological Properties. *J. Mater. Chem.*. **2012**, *22*, 895−902.
(32) Senatore, A.; D'Agostino, V.; Petrone, V.; Ciambelli, P.; Sarno, M. Graphene Oxide Nanosheets as Effective Friction Modifier for Oil Lubricant: Materials, Methods, and Tribological Results. *ISRN Tribology.* **2013**, 1−9.
(33) Wu, Y. Y.; Tsui, W. C.; Liu, T. C. Experimental Analysis of Tribological Properties of Lubricating Oils with Nanoparticle Additives. *Wear* **2007**, *262*, 819−825.

DOI: 10.1021/acsami.5b02650
ACS Appl. Mater. Interfaces 2015, 7, 11604−11612